

Cite this: *Sustainable Energy Fuels*,
2024, 8, 1944Received 26th January 2024
Accepted 16th March 2024

DOI: 10.1039/d4se00146j

rsc.li/sustainable-energy

Sequential proton coupled electron transfer events from a tetraruthenium polyoxometalate in photochemical water oxidation†

Elena Rossin,^{id}^a Marcella Bonchio,^{id}^a Mirco Natali^{id}^{*b} and Andrea Sartorel^{id}^{*a}

The tetraruthenium polyoxometalate $\{\text{Ru}^{\text{IV}}(\text{H}_2\text{O})_4(\mu\text{-OH})_2(\mu\text{-O})_4[\text{SiW}_{10}\text{O}_{36}]_2\}^{10-}$ (Ru_4POM) shows multiple oxidative proton coupled electron transfer (PCET) events in a $[\text{Ru}(\text{bpy})_3]^{2+}/\text{S}_2\text{O}_8^{2-}$ photochemical cycle for catalytic water oxidation, with electrons conveyed to the photogenerated $[\text{Ru}(\text{bpy})_3]^{3+}$ oxidant and protons transferred to aqueous bases. As shown by laser flash photolysis, in aqueous phosphate buffer the consumption of the $[\text{Ru}(\text{bpy})_3]^{3+}$ oxidant by Ru_4POM shows bi-exponential kinetics with a fast component and a slow component that feed the Ru_4POM catalyst with up to 6 oxidative equivalents through PCET in ca. 50 ms. The apparent rates of both the fast and slow components depend linearly on HPO_4^{2-} and on the pH of the aqueous medium, suggesting the involvement of the buffer base, of water and of OH^- in assisting removal of the protons from Ru_4POM . In particular, the beneficial role of HPO_4^{2-} is reflected in a proportional improvement in the oxygen evolution activity, reaching quantum efficiency approaching 14%, although an excessive increase of buffer concentration is detrimental to the $[\text{Ru}(\text{bpy})_3]^{3+}$ stability and leads to the abatement of the O_2 evolution.

Introduction

Proton coupled electron transfer (PCET) is a pervasive process in many biological and artificial chemical transformations.^{1–4} PCET events are often associated with photoinduced charge separation,^{5–10} which is a primary step in chemical processes associated with the photosynthetic conversion of small molecules, while recently, its interest has broadened to synthetic organic chemistry.^{11–15}

In the field of water oxidation, investigation of PCET was pioneered by T. J. Meyer, who recognized that for the $[\text{Ru}^{\text{II}}(\text{H}_2\text{O})(\text{py})(\text{bpy})_2]^{2+}$ coordination complex (where py = pyridine; bpy = 2,2'-bipyridine) two stepwise oxidative PCET events occurring in a narrow potential window of 110 mV lead to the formation of a Ru^{IV} -oxo species;¹⁶ these findings were pivotal in the design of the blue dimer $[(\text{bpy})_2\text{Ru}^{\text{III}}(\text{H}_2\text{O})(\mu\text{-O})\text{Ru}^{\text{III}}(\text{H}_2\text{O})(\text{bpy})_2]^{4+}$ as the first molecular water oxidation catalyst.¹⁷ The importance of PCET was then recognised in many ruthenium based catalytic manifolds,^{18–22} including the case of the tetraruthenium polyoxometalate $\{\text{Ru}^{\text{IV}}(\text{H}_2\text{O})_4(\mu\text{-OH})_2(\mu\text{-O})_4[\text{SiW}_{10}\text{O}_{36}]_2\}^{10-}$ (Ru_4POM) investigated in this work (Scheme 1). Ru_4POM is the first structurally characterized polyoxometalate based water

oxidation catalyst,^{23,24} and has been extensively investigated in electrochemical,^{25,26} photochemical^{27,28} and photo-electrochemical systems;^{29–32} its tetraruthenium active core $[\text{Ru}^{\text{IV}}(\text{H}_2\text{O})_4(\mu\text{-OH})_2(\mu\text{-O})_4]^{6+}$ can indeed undergo stepwise oxidation processes associated with the formation of high-valent intermediates characterised spectroscopically or with computational tools, up to the formation of Ru–oxo moieties active towards oxygen evolution at low overpotential.

Despite ruthenium catalysts being reported to show excellent performance in oxygenic photosynthetic systems,^{18,33–35} the



Scheme 1 Multiple and sequential proton coupled electron transfer events from a tetraruthenium polyoxometalate Ru_4POM to photo-generated $[\text{Ru}(\text{bpy})_3]^{3+}$ investigated in this work through laser flash photolysis, with HPO_4^{2-} , H_2O and OH^- being responsible for proton transfer.

^aDepartment of Chemical Sciences, University of Padova, Via Marzolo 1, 35131 Padova, Italy. E-mail: Andrea.sartorel@unipd.it

^bDepartment of Chemical Pharmaceutical and Agricultural Sciences (DOCPAS), University of Ferrara, Ferrara, Italy. E-mail: Mirco.natali@unife.it

† Electronic supplementary information (ESI) available. See DOI: <https://doi.org/10.1039/d4se00146j>



managing of the necessary PCET events under photochemical conditions has been poorly investigated. Moreover, most of the PCET studies in photosynthetic systems for water oxidation refer to a single event,³³ and thus represent only the primary step in the water oxidation process.

In this study, we report multiple, sequential oxidative PCET events from Ru₄POM to a photogenerated [Ru(bpy)₃]³⁺ oxidant (electron acceptor) highlighting the role of bases as the proton acceptors (Scheme 1). We will show by laser flash photolysis studies that the nature and concentration of the buffer impact the dynamics and the number of oxidation processes at the Ru₄POM catalyst, showing a consistent effect in the O₂ evolving rate.

Results and discussion

Primary electron transfer from Ru₄POM to [Ru(bpy)₃]³⁺

In the laser flash photolysis set-up, [Ru(bpy)₃]³⁺ is photo-generated in a few ns upon laser excitation ($\lambda_{\text{exc}} = 355 \text{ nm}$) of a solution containing the [Ru(bpy)₃]²⁺ sensitizer and the S₂O₈²⁻ sacrificial acceptor (a quantum yield of 2 is reported for Ru(III) formation, since two equivalents of Ru(III) are generated upon one photon absorption according to the reaction steps in Scheme S1 in ESI†). Formation of Ru(III) is confirmed by the decrease of the absorbance at 450 nm (usually referred to as “bleach”, Fig. 1).

In the presence of Ru₄POM, the Ru(II) initial absorption is restored in a few μs (“bleach recovery”, Fig. 1), indicating consumption of the [Ru(bpy)₃]³⁺ oxidant by Ru₄POM, thus leading to the formation of the singly oxidized form of the Ru₄POM catalyst, Ru₄POM^{ox}.‡

Under pseudo first order conditions with [Ru₄POM] \gg [[Ru(bpy)₃]³⁺], fitting of the bleach recovery traces leads to the determination of the bimolecular rate constant k_I for the primary oxidative process in Ru₄POM (eqn (1)), involving oxidation of one Ru^{IV}-OH₂ moiety into Ru^V-OH.



In order to map the possible involvement of a PCET event in this primary step, we performed the laser flash photolysis investigation in aqueous solutions at different pH values (in the range 2–7, conditions associated with the stability of Ru₄POM in aqueous solution) employing different buffer and buffer concentrations. In Fig. 1, traces correspond to phosphate buffer at pH 7, while traces under other reaction conditions are reported in ESI (Fig. S1–S4).†

The main outcome of this analysis is that the primary oxidation of Ru₄POM by [Ru(bpy)₃]³⁺ occurs under diffusion

‡ In all the experiments, 0.1 M Na₂SO₄ was employed to guarantee a sufficient ionic strength of the medium ($I = 0.3 \text{ M}$), thus mitigating: (a) formation of [Ru(bpy)₃]²⁺·Ru₄POM ion pairs, where fast static quenching of the [Ru(bpy)₃]²⁺ photosensitizer hampers the occurrence of the envisaged photosynthetic cycle,²⁷ and (b) ET rate constant variability associated with the change of the ionic strength due to the change of buffer concentrations; the rate constant for a diffusion based ET event between charged reactants (as in the present case) is sensitive to the ionic strength according to the Debye–Eigen theory.⁴⁹

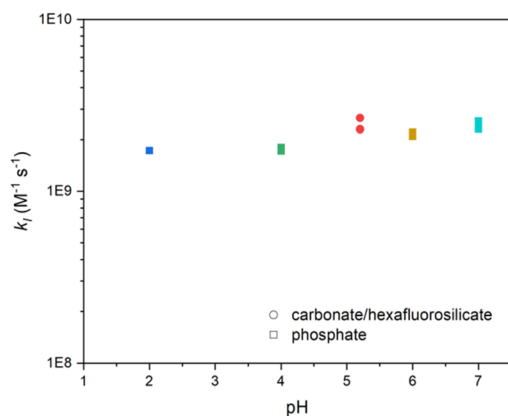
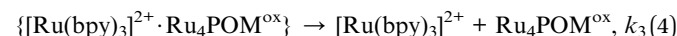
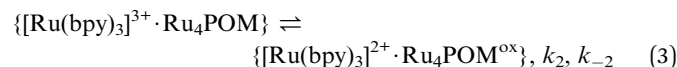


Fig. 1 (Top panel) Kinetic traces at 450 nm obtained by laser flash photolysis of 50 μM Ru(bpy)₃Cl₂, 5 mM Na₂S₂O₈, 30 μM Na₁₀Ru₄POM, 0.1 M Na₂SO₄ in 5–50 mM phosphate buffer at pH 7.0. (Medium panel) Bimolecular rate constant k_I (in logarithmic scale) for the primary oxidation of Ru₄POM by [Ru(bpy)₃]³⁺ vs. pH (the different data at a specific pH refer to the different concentrations of the buffer employed). (Bottom panel) k_I (in logarithmic scale) vs. buffer base concentration for all experimental conditions tested (the different colours refer to the conditions employed, with the base specified in brackets in the legend panel).

control under all the conditions explored (k_I in the range $1.7 \div 2.5 \times 10^9 \text{ M}^{-1} \text{ s}^{-1}$).²⁷ The classical model for bimolecular ET reactions foresees the formation of the {[Ru(bpy)₃]³⁺·Ru₄POM}



encounter complex, eqn (2), followed by ET to form the successor complex $\{[\text{Ru}(\text{bpy})_3]^{2+} \cdot \text{Ru}_4\text{POM}^{\text{ox}}\}$, eqn (3), and product diffusion, eqn (4); assuming a steady state condition for the encounter and successor complexes the equation of the rate constant k_I can be expressed by eqn (5).³⁶



$$k_I = \frac{k_1}{[1 + (1 + k_{-2}/k_3) \times k_{-1}/k_2]} \quad (5)$$

A diffusion limited k_I is expected when both $k_3 \gg k_{-2}$ and $k_2 \gg k_{-1}$, in which case $k_I \approx k_1$; this occurs under all the conditions explored for the process in eqn (1). This is beneficial towards the accumulation of the first oxidation equivalent in $\text{Ru}_4\text{POM}^{\text{ox}}$ (*i.e.* backward processes do not significantly compete with forward processes in eqn (2)–(4)), but limits a mechanistic comprehension of the Ru_4POM to $\text{Ru}_4\text{POM}^{\text{ox}}$ conversion, according to the expected PCET event from electrochemistry data.³⁷

We then focused our analysis on multiple accumulation of oxidation equivalents in Ru_4POM by photogenerated $[\text{Ru}(\text{bpy})_3]^{3+}$.

Multiple electron transfer events from Ru_4POM to $[\text{Ru}(\text{bpy})_3]^{3+}$: effect of pH, buffer, and buffer concentration

The fast accumulation of oxidation equivalents in Ru_4POM by photogenerated $[\text{Ru}(\text{bpy})_3]^{3+}$ can be investigated by performing flash photolysis experiments using a low concentration of Ru_4POM to guarantee $[\text{Ru}_4\text{POM}] \ll [[\text{Ru}(\text{bpy})_3]^{3+}]$ conditions.²⁷ With this setup, the amount of bleach recovery is associated with the number n of ET events from Ru_4POM to $[\text{Ru}(\text{bpy})_3]^{3+}$ occurring in the timeframe of the experiment (50 ms), and generating a multiply oxidized form of the catalyst (eqn (6)), while the single steps can be represented as in eqn (7).



Experiments aimed at tracing multiple electron transfer events were conducted under aqueous conditions at different pH, buffer, and buffer concentrations. A representative example is shown in Fig. 2 (pH 7, 5–100 mM phosphate buffer), see ESI† for other traces (Fig. S5–S7†). The initial concentration of photochemically generated $[\text{Ru}(\text{bpy})_3]^{3+}$ in Fig. 2 (top panel) is *ca.* 2×10^{-5} M and is obtained from the $\Delta(\text{OD})^{450}$ abatement;[§]

§ The photogenerated concentration of $[\text{Ru}(\text{bpy})_3]^{3+}$ is calculated from $\Delta\epsilon^{450}(\text{Ru}(\text{n})/\text{Ru}(\text{m})) = 1.3 \times 10^4 \text{ M}^{-1} \text{ cm}^{-1}$ and the appropriate correction for the ratio between the volume of solution probed by the analysing beam and that excited by the laser pulse (1.35, as obtained from saturation techniques). As a result, a $\Delta(\text{OD})$ of 0.1 corresponds to a concentration of photogenerated $[\text{Ru}(\text{bpy})_3]^{3+}$ of 1.04×10^{-5} M.

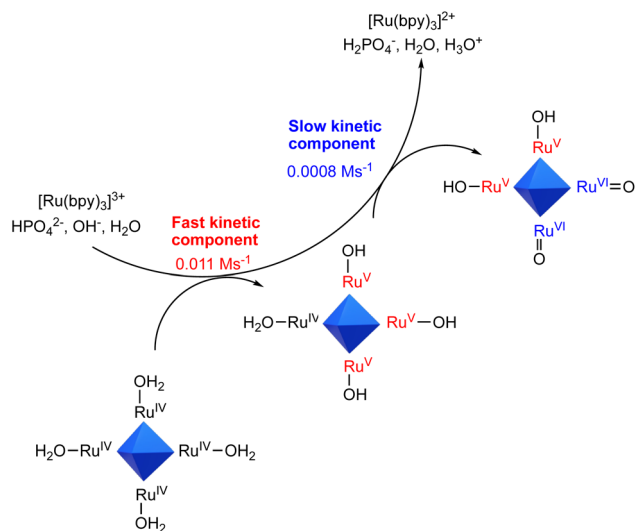


Fig. 2 (Top panel) Kinetic traces at 450 nm obtained by laser flash photolysis of 100 μM $\text{Ru}(\text{bpy})_3\text{Cl}_2$, 5 mM $\text{Na}_2\text{S}_2\text{O}_8$, 2.5 μM $\text{Na}_{10}\text{Ru}_4\text{POM}$, 0.1 M Na_2SO_4 in unbuffered water and in 5–100 mM phosphate buffer at pH 7.0. The solid lines indicate the biexponential fittings of the traces (monoexponential fitting in the trace in water). (Bottom panel) Plot of the number of $\text{Ru}_4\text{POM} \rightarrow [\text{Ru}(\text{bpy})_3]^{3+}$ ET events in 50 ms vs. the concentration of HPO_4^{2-} (base of the buffer). The number of ET events is estimated from the experimental recovery of the bleach in the kinetic traces in the top panel. The error bars are given as semi-dispersion of two separate experiments.

considering the concentration of 2.5 μM of Ru_4POM employed in the experiment, the traces indicate that the amount of $[\text{Ru}(\text{bpy})_3]^{3+}$ being reduced by Ru_4POM actually exceeds the amount of Ru_4POM and shows a dependence on the buffer concentration. The role of Ru_4POM in the reactivity of $[\text{Ru}(\text{bpy})_3]^{3+}$ was confirmed by conducting experiments by varying the concentration of Ru_4POM (in the range 0.5–2.5 μM) and keeping the buffer concentration constant at 100 mM: the amount of $\Delta(\text{OD})$ recovery of $[\text{Ru}(\text{bpy})_3]^{3+}$ depends linearly on Ru_4POM concentration (Fig. S8 in ESI† and further discussion).

These results speak in favour of the occurrence of multiple PCET events from Ru_4POM , with the HPO_4^{2-} base of the buffer being responsible for the transfer of the protons, while electrons are conveyed to $[\text{Ru}(\text{bpy})_3]^{3+}$. The number of ET events increases up to a HPO_4^{2-} base concentration of *ca.* 15 mM, above which a plateau value of *ca.* 6 events is reached (Fig. 2, bottom panel). This concentration threshold is likely due to the availability of the





Scheme 2 Schematic representation of the accumulation of oxidation equivalents on Ru₄POM through sequential PCET involving [Ru(bpy)₃]³⁺ and aqueous bases within two kinetic regimes.

HPO₄²⁻ base in proximity of the Ru₄POM site reacting through PCET. Indeed, in the case of Ru₄POM, accumulation of 6 oxidizing equivalents is associated with the generation of Ru^{VI}oxo states through Ru^{IV}(H₂O)/Ru^V(OH)/Ru^{VI}(O) manifolds, subjected to a water nucleophilic attack as the first step finally releasing dioxygen in the catalytic cycle (Scheme 2).³⁸

In order to extract kinetic parameters from the experimental traces in Fig. 2 we focused on the profile of consumption of [Ru(bpy)₃]³⁺ and used bi-exponential functions to describe the recovery of the Δ(OD) along the experiments, (eqn (8)):[¶]

$$\Delta(\text{OD}) = -A_{\text{F}} \times \exp(-t/\tau_{\text{F}}) - A_{\text{S}} \times \exp(-t/\tau_{\text{S}}) + \Delta(\text{OD})_{@50\text{ms}} \quad (8)$$

where τ_F and τ_S indicate a fast and a slow time constant, respectively, A_F and A_S indicate the amplitudes of the two components in the Δ(OD) recovery (Table 1), while Δ(OD)_{@50ms} is the residual Δ(OD) value after 50 ms.

First, it is interesting to note that the relative amplitude contributions of the fast and slow components to the reactivity of [Ru(bpy)₃]³⁺ depend on the concentration of the buffer base (Fig. 3 top panel). The relative contributions of the fast and slow components – calculated as A_F × 100/(A_F + A_S) and A_S × 100/(A_F + A_S), respectively – at low HPO₄²⁻ concentrations are indeed 33% and 67%, respectively, while at high HPO₄²⁻ concentrations the relative contributions reach plateau values of 45% and 55% for the fast and slow components, respectively.

[¶] In this case, a biexponential function was necessary to provide a suitable fitting of the experimental data. The use of a biexponential function to fit the traces where six sequential oxidation processes are postulated can be explained considering the similar reaction rates of the Ru₄POM oxidized intermediates with [Ru(bpy)₃]³⁺. This is indeed not unexpected taking into account the close spacing in potential associated with the oxidation of Ru₄POM according to electrochemical studies.³⁷ The use of multiexponential functions is often exploited in the case of electron transfer involving metal oxide particles, due to the presence of surface sites with different reactivity.³⁹

From the fitting parameters we then derived two apparent rates for the reactivity of [Ru(bpy)₃]³⁺ with Ru₄POM due to the fast and slow components (eqn (9) and (10); the 1.04 × 10⁻⁴ factor converts the Δ(OD) units of A_F and A_S into the corresponding concentration of [Ru(bpy)₃]³⁺):^{||}

$$\text{App. Rate}_{\text{Fast}} (\text{M s}^{-1}) = A_{\text{F}}/\tau_{\text{F}} \times 1.04 \times 10^{-4} \quad (9)$$

$$\text{App. Rate}_{\text{Slow}} (\text{M s}^{-1}) = A_{\text{S}}/\tau_{\text{S}} \times 1.04 \times 10^{-4} \quad (10)$$

As shown in Fig. 3 (bottom panel and inset), the apparent rates determined above depend linearly on the concentration of the HPO₄²⁻ base of the phosphate buffer (the log–log plot analysis supports a first order in [HPO₄²⁻] in both apparent rates, see ESI Fig. S10[†]).

$$\text{App. Rate}_{\text{Fast}} (\text{M s}^{-1}) = 2.62 \times 10^{-3} + 2.04 \times 10^{-4} [\text{HPO}_4^{2-}] \quad (11)$$

$$\text{App. Rate}_{\text{Slow}} (\text{M s}^{-1}) = 5.45 \times 10^{-4} + 6.38 \times 10^{-6} [\text{HPO}_4^{2-}] \quad (12)$$

The linear dependence of the rates on [HPO₄²⁻] confirms the role of the base in assisting the removal of the protons from Ru₄POM along its conversion to highly oxidized states through reactivity with [Ru(bpy)₃]³⁺ (both apparent rates are indeed linearly dependent on Ru₄POM concentration, see Fig. S11[†]).

For both the fast and slow apparent rates, the non-null intercept in eqn (11) and (12) indicates that HPO₄²⁻ is not the only base assisting the reactivity of [Ru(bpy)₃]³⁺ towards Ru₄POM. When conducting the analysis at lower pH (100 mM phosphate buffer pH 6) a significant abatement of both components of apparent rates was observed,^{**} Table 1 and Fig. 3, medium and bottom panels. Registration and fitting of a trace in water in the absence of any buffer (in this case through a monoexponential fitting) lead to the obtainment of a single component of the apparent rate, which was significantly abated with respect to the values previously determined. These results indicate that both OH⁻ and H₂O are involved in the reactivity of [Ru(bpy)₃]³⁺ towards Ru₄POM (Scheme 2).^{36,39††} The possibility for a base to assist PCET events is associated with the libido rule^{40,41} and with the strength of the base, expressed in terms of the pK_a of the conjugate acid/base couples (in this case: pK_a = 7.2 for H₂PO₄⁻/HPO₄²⁻, pK_a = 0 for H₃O⁺/H₂O, pK_a = 14 for H₂O/OH⁻). Although H₂O is the least basic, the possibility of preorganisation of water channels at the

^{||} An alternative analysis considers the determination of an average time constant (τ) = (A_F × τ_F + A_S × τ_S)/(A_F + A_S), and the determination of average apparent rates as: App. Rate_{Average} (M⁻¹ s⁻¹) = (A_F + A_S)/(τ) × 1.04 × 10⁻⁴. This leads to a consistent dependence of the average App. Rate on [HPO₄²⁻], see ESI (Fig. S9 and Table S1).[†]

^{**} At pH 6 (phosphate buffer), investigation of other buffer concentrations leads to a marked abatement of [Ru(bpy)₃]³⁺ recovery, thus hampering the possibility of exploring further the system. Reasonable data and fittings were obtained only for the conditions reported in the main text.

^{††} The consumption of [Ru(bpy)₃]³⁺ by Ru₄POM in the absence of buffer base could also be consistent with a stepwise mechanism ET/PT, in which electron transfer precedes proton transfer.



Table 1 Fitting parameters according to eqn (8) for the traces in Fig. 2, top and medium panels. A_F and A_S are the intensity of $\Delta(\text{OD})$ recovery associated with the fast and slow components, respectively, and can be converted into the total concentration of consumed $[\text{Ru}(\text{bpy})_3]^{3+}$ multiplying them by a 1.04×10^{-4} M factor, see footnote §

Different pH and phosphate buffer concentrations ^a				
pH ([buffer], mM)	A_F (τ_F , ms)	A_S (τ_S , ms)	App. Rate _{Fast} $\times 10^3$, M s ⁻¹	App. Rate _{Slow} $\times 10^3$, M s ⁻¹
7 (5)	0.025 \pm 0.001 (0.85 \pm 0.04)	0.051 \pm 0.004 (9.7 \pm 0.1)	3.12 \pm 0.19	04.54 \pm 0.04
7 (10)	0.034 \pm 0.001 (0.99 \pm 0.06)	0.060 \pm 0.001 (10.7 \pm 0.2)	3.56 \pm 0.24	0.58 \pm 0.01
7 (20)	0.045 \pm 0.001 (1.05 \pm 0.04)	0.063 \pm 0.004 (10.7 \pm 0.2)	4.43 \pm 0.19	0.61 \pm 0.04
7 (50)	0.051 \pm 0.001 (0.92 \pm 0.05)	0.062 \pm 0.001 (10.1 \pm 0.2)	5.75 \pm 0.33	0.64 \pm 0.02
7 (100)	0.060 \pm 0.002 (0.57 \pm 0.03)	0.069 \pm 0.001 (8.9 \pm 0.1)	10.87 \pm 0.67	0.80 \pm 0.02
6 (100)	0.036 \pm 0.001 (2.15 \pm 0.12)	0.035 \pm 0.001 (11.6 \pm 0.5)	1.73 \pm 0.11	0.31 \pm 0.01
Water	0.022 \pm 0.001 (4.0 \pm 0.1)	—	0.56 \pm 0.02	—

Different concentrations of Ru ₄ POM (Fig. S8) ^b				
[Ru ₄ POM] μM	A_F (τ_F , ms)	A_S (τ_S , ms)	App. Rate _{Fast} $\times 10^3$, M s ⁻¹	App. Rate _{Slow} $\times 10^3$, M s ⁻¹
2.5	0.060 \pm 0.002 (0.57 \pm 0.02)	0.069 \pm 0.001 (8.9 \pm 0.1)	10.87 \pm 0.67	0.80 \pm 0.20
1	0.043 \pm 0.001 (1.29 \pm 0.05)	0.058 \pm 0.001 (9.7 \pm 0.2)	3.44 \pm 0.13	0.62 \pm 0.17
0.5	0.038 \pm 0.002 (3.05 \pm 0.16)	0.039 \pm 0.002 (13.7 \pm 0.6)	1.30 \pm 0.10	0.30 \pm 0.20

^a 100 μM Ru(bpy)₃Cl₂, 5 mM Na₂S₂O₈, 2.5 μM Na₁₀Ru₄POM, 0.1 M Na₂SO₄ in 5–100 mM phosphate buffer at pH 7.0, 100 mM phosphate buffer pH 6.0 or water. ^b 100 μM Ru(bpy)₃Cl₂, 5 mM Na₂S₂O₈, 0.5–2.5 μM Na₁₀Ru₄POM, 0.1 M Na₂SO₄ in 100 mM phosphate buffer at pH 7.0. In all cases the photogenerated $[\text{Ru}(\text{bpy})_3]^{3+}$ estimated from the initial $\Delta(\text{OD})$ is ca. 20 μM .

hydrophilic surface of polyoxometalates may favour its role in assisting the transfer of protons during oxidation of Ru₄POM.³⁶ Finally, superimposable kinetic traces and unchanged fitting parameters were obtained when registering the experiment in deuterated medium (Fig. S12 in ESI,[†] obtained by laser flash photolysis of 100 μM Ru(bpy)₃Cl₂, 5 mM Na₂S₂O₈, 2.5 μM Na₁₀Ru₄POM, 0.1 M Na₂SO₄ in 100 mM deuterated phosphate buffer at pD 7.0), indicating a negligible H/D isotopic effect in the multiple ET dynamics. In single PCET events, small H/D isotope effects are indicative of a low modification of the overlap integrals of the donor–acceptor states along the proton transfer coordinate, when replacing H with D.⁴²

The whole mechanistic scenario is represented in Scheme 2, where $[\text{Ru}(\text{bpy})_3]^{3+}$ feeds Ru₄POM with 6 oxidizing equivalents up to Ru^{VI}=O states, with the assistance of aqueous bases in two distinct kinetic regimes. We finally attempted to estimate rate constants for the stepwise PCET processes by employing a kinetic model that considers 6 consecutive bimolecular events involving $[\text{Ru}(\text{bpy})_3]^{3+}$ and Ru₄POM (previous eqn (7)), each one associated with a bimolecular rate constant k_j ($j = 1$ –6). Under the optimal conditions investigated (100 mM phosphate buffer, pH 7, purple trace in Fig. 2 top panel), the fitting provides values in the range $1.3 \times 10^8 \div 2 \times 10^9 \text{ M}^{-1} \text{ s}^{-1}$ for k_1 – k_3 (associated with the fast component of the reactivity of $[\text{Ru}(\text{bpy})_3]^{3+}$ and with the generation of the primary oxidized intermediates of Ru₄POM) and $1.2 \times 10^7 \div 4.5 \times 10^7 \text{ M}^{-1} \text{ s}^{-1}$ for k_4 – k_6 (associated with the slow component of the reactivity of $[\text{Ru}(\text{bpy})_3]^{3+}$ and with the generation of the highly oxidized intermediates of Ru₄POM). The slowing down of the rate for reaching highly oxidized Ru₄POM intermediates is expected based on less

favorable thermodynamics, according to the higher potentials associated with such species.^{37,38†‡}

Impact of the PCET mechanism in light driven O₂ evolution

We finally investigated the implication of the PCET mechanism and the effect of the buffer concentration on the O₂ evolution of the system, by irradiating 15 mL of an aqueous buffered solution containing 0.1 M Na₂SO₄, 1 mM Ru(bpy)₃Cl₂, 5 mM Na₂S₂O₈ and 5 μM of Na₁₀Ru₄POM with a blue LED ($\lambda_{\text{em}} = 450 \text{ nm}$, FWHM 10 nm). The O₂ evolution traces are reported in Fig. 4, and show an initial linear production of O₂, before reaching a plateau after 1–2 h irradiation. The key performance indicators are collected in Table 2; in this case, we considered the maximum O₂ evolving rate, Rate(O₂)_{MAX}, as the most significant one to evaluate the efficiency of the system and the effect of the buffer concentration. The main outcome can be summarised as follows:

(i) The system shows O₂ evolution activity also in the absence of buffer, with a Rate(O₂)_{MAX} of $6.56 \times 10^{-4} \mu\text{mol}(\text{O}_2) \text{ s}^{-1}$; upon addition of the phosphate buffer (5–10 mM), an increase in Rate(O₂)_{MAX} is observed up to $1.61 \times 10^{-3} \mu\text{mol}(\text{O}_2) \text{ s}^{-1}$ (Fig. 4 bottom panel; for consistency with previous data, we reported the HPO₄²⁻ base concentration in the abscissa). In oxygen evolution, the effect of the buffer can be related to multiple factors, including the aid in generating oxidized intermediates of the catalyst (*vide supra*), assisting the water nucleophilic attack and the oxygen–oxygen bond formation,³⁸ managing the protons released in the water oxidation process.

†† The kinetic model considering 6 consecutive oxidative events was applied also for the other experimental traces in the Fig. 2 top panel, but in these cases it led to overfitting of the data, see details in ESI.[†]



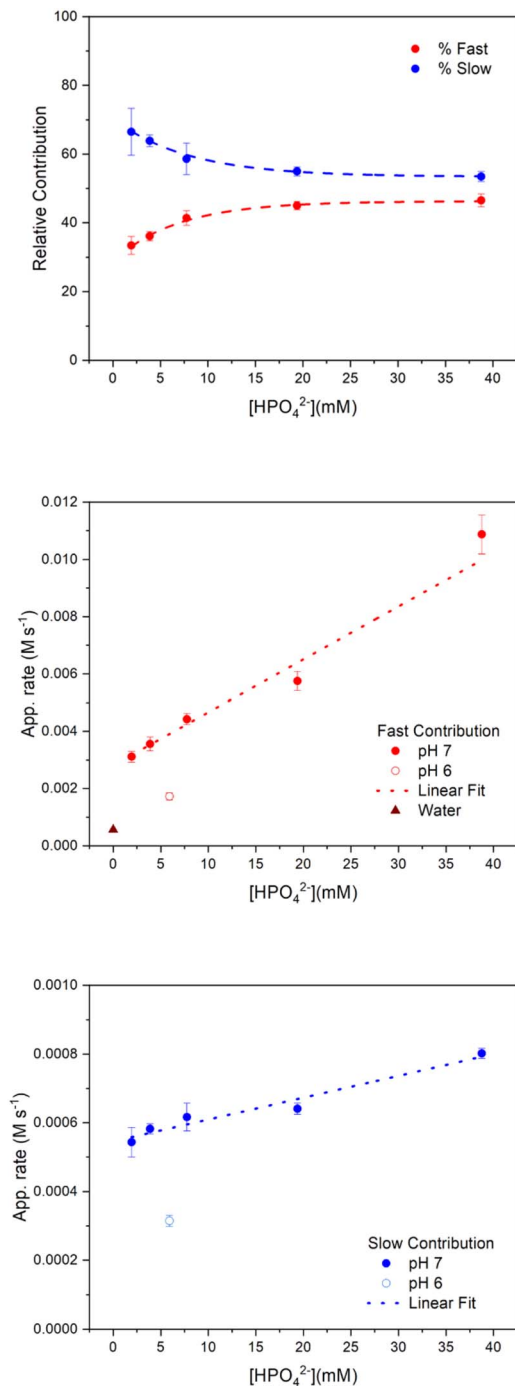


Fig. 3 (Top panel) Relative contribution of the two components to the recovery of the traces, calculated as $A_F \times 100 / (A_F + A_S)$ and $A_S \times 100 / (A_F + A_S)$, respectively. (Medium panel) Plot of apparent rates for $[\text{Ru}(\text{bpy})_3]^{3+}$ consumption vs. the concentration of base of the buffer for the fast contribution at different pH. (Bottom panel) Plot of apparent rates for $[\text{Ru}(\text{bpy})_3]^{3+}$ consumption vs. the concentration of base of the buffer for the slow contribution at different pH.

(ii) A further increase of buffer concentration in the reaction conditions leads to a progressive abatement of $\text{Rate}(\text{O}_2)_{\text{MAX}}$ (Fig. 4). This effect is ascribed to a rapid deactivation of the $[\text{Ru}(\text{bpy})_3]^{2+}$ photosensitizer,^{43–45} confirmed by UV-vis analysis of the reaction solution, which visibly turns from brilliant orange

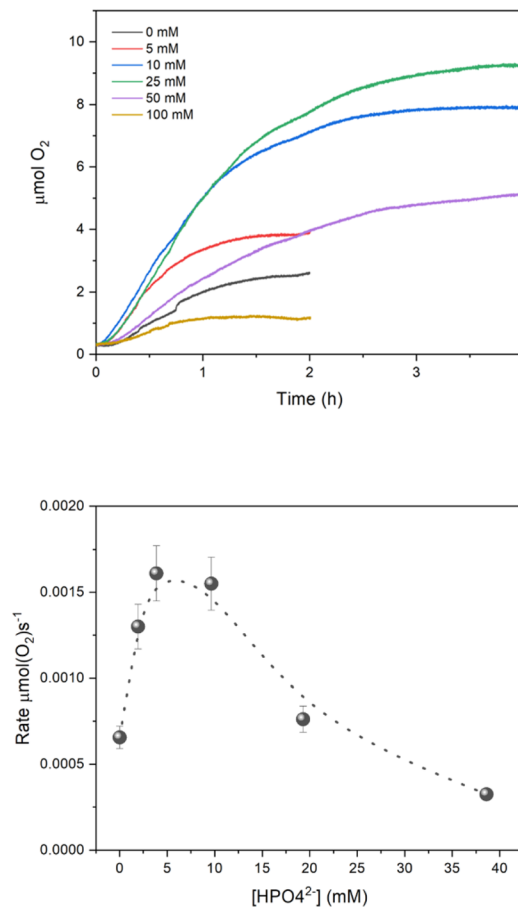


Fig. 4 (Top panel) O_2 evolution kinetics (see Table 2 for conditions). (Bottom panel) Plot of $\text{Rate}(\text{O}_2)_{\text{MAX}}$ vs. the concentration of HPO_4^{2-} buffer base. Error bars result from repetitive runs.

to brownish along the first minutes of irradiation (Fig. S13†). Recently, two decomposition pathways were elucidated for $[\text{Ru}(\text{bpy})_3]^{2+}$ when combined with light and persulfate: a dark one, occurring at $\text{pH} > 6$, in which photogenerated $[\text{Ru}(\text{bpy})_3]^{3+}$ reacts with OH^- to form OH^\bullet radicals which then attack the bpy ligands, and a light-induced one, starting from excitation of the $[\text{Ru}(\text{bpy})_3]^{3+}$ oxidised state, promoting its reactivity with $\text{S}_2\text{O}_8^{2-}$.⁴⁵ Given the specific conditions employed in our study ($\text{pH} 7$, irradiation at 450 nm corresponding to the MLCT band of $[\text{Ru}(\text{bpy})_3]^{2+}$) it is plausible that the dark decomposition pathway prevails, with HPO_4^{2-} being also involved in the radical reactivity.⁴⁶ Detrimental effects of high buffer concentration in water oxidation catalysis were previously documented under both light driven³⁹ and electrochemical conditions.⁴⁷

(iii) Finally, under the optimized buffer conditions (10 mM), we explored the effect of light intensity on O_2 generation. When reducing the photon flux from 8.28×10^{-8} to 3.33×10^{-8} and to 0.87×10^{-8} einstein s^{-1} , a progressive decrease of $\text{Rate}(\text{O}_2)_{\text{MAX}}$ was observed from 1.61×10^{-3} to 1.16×10^{-3} and to 5.93×10^{-4} $\mu\text{mol}(\text{O}_2) \text{s}^{-1}$, indicative of light being a limiting reagent (Fig. S14†). Lowering the light intensity leads to an optimization of photon exploitation, as demonstrated by the quantum yield $\phi(\text{O}_2)$ of the process reaching 6.8; this corresponds to a quantum efficiency for oxygen evolution of 13.6%, given that



Table 2 Key performance parameters of the O₂ evolution kinetics. General conditions: 15 mL of an aqueous solution containing 0.1 M Na₂SO₄, 1 mM Ru(bpy)₃Cl₂, 5 mM Na₂S₂O₈ and 5 μM of Na₁₀Ru₄POM. Irradiation with a blue LED (λ_{em} = 450 nm, FWHM 10 nm), photon flux = 8.28 × 10⁻⁸ einstein s⁻¹. The maximum rate is evaluated from a linear fitting of the initial part of the traces (between 10 and 30 minutes). Turnover frequency (TOF) and turnover numbers (TONs) are calculated with respect to Ru₄POM

[Buffer] mM	Rate(O ₂) _{MAX} μmol(O ₂) s ⁻¹	TOF × 10 ² s ⁻¹	μmol(O ₂)	TON	QE%
—	6.56 × 10 ⁻⁴	0.87 ± 0.1	2.8 ± 0.3	37 ± 3	1.6 ± 0.2
5	1.30 × 10 ⁻³	1.73 ± 0.1	4.3 ± 0.4	57 ± 6	3.2 ± 0.2
10	1.61 × 10 ⁻³	2.15 ± 0.2	8.0 ± 0.8	107 ± 9	3.8 ± 0.4
25	1.55 × 10 ⁻³	2.07 ± 0.2	9.5 ± 0.9	127 ± 12	3.8 ± 0.4
50	7.62 × 10 ⁻⁴	1.02 ± 0.1	5.1 ± 0.5	68 ± 6	1.8 ± 0.2
100	3.24 × 10 ⁻⁴	0.43 ± 0.04	1.2 ± 0.1	16 ± 1	0.8 ± 0.1
10 ^a	1.16 × 10 ⁻³	1.55 ± 0.1	8.4 ± 0.8	112 ± 11	6.8 ± 0.6
10 ^b	5.93 × 10 ⁻⁴	0.79 ± 0.1	6.4 ± 0.6	85 ± 8	13.6 ± 1.2

^a Photon flux = 3.33 × 10⁻⁸ einstein s⁻¹. ^b Photon flux = 0.87 × 10⁻⁸ einstein s⁻¹.

a theoretical maximum quantum yield φ(O₂) = 0.50 is expected with the [Ru(bpy)₃]²⁺/S₂O₈²⁻ cycle, where the production of one oxygen molecule theoretically requires the absorption of two photons (see Scheme S1 in ESI†).⁴⁸ A value of 9% for quantum efficiency was previously reported in the literature under similar reaction conditions but with 420–520 nm irradiation.²⁸

Conclusions and perspectives

We investigated the accumulation of oxidizing equivalents on the Ru₄POM water oxidation catalyst through PCET events in a [Ru(bpy)₃]²⁺/S₂O₈²⁻ photochemical cycle. Laser flash photolysis experiments indicate the occurrence of 6 oxidative PCET events on Ru₄POM in *ca.* 50 ms, leading to the generation of competent Ru^{VI}-oxo intermediates. While electrons are conveyed from Ru₄POM to the [Ru(bpy)₃]³⁺ oxidant, protons are transferred to aqueous bases. The flash photolysis traces show indeed two components of the rate of [Ru(bpy)₃]³⁺ reactivity, both linearly dependent on the HPO₄²⁻ buffer base concentration; a contribution of H₂O and OH⁻ in managing protons was also highlighted. The effect of HPO₄²⁻ buffer base was evident also in O₂ evolving kinetics, inducing a progressive increase of O₂ rate up to 5–10 mM, above which the system loses activity due to [Ru(bpy)₃]²⁺ photosensitizer fast decomposition. Under optimal buffer composition, managing light intensity led to reaching a quantum efficiency up to 13.6%.

This work highlights the importance of considering the molecular nature of PCET events under photochemical conditions, since this can significantly impact the efficiency of the overall process. The investigation of this aspect is expected to be general and broad, given the fact that PCET events are pervasive in many chemical transformations.

Experimental part

Instrumentation and procedures

Na₁₀{Ru^{IV}(H₂O)₄(μ-OH)₂(μ-O)₄[SiW₁₀O₃₆]₂} (Na₁₀Ru₄POM) was synthesised as previously reported.^{29–31}

Nanosecond transient absorption measurements were performed with a custom laser spectrometer consisting of

a Continuum Surelite II Nd:YAG laser (FWHM 6–8 ns) with an option to double (532 nm) or triple (355 nm) the frequency, an Applied Photo-physics xenon light source including a mod. 720 150 W lamp housing, a mod. 620 power-controlled lamp supply and a mod. 03-102 arc lamp pulser. Laser excitation was provided at 90° with respect to the white light probe beam. Light transmitted by the sample was focused onto the entrance slit of a 300 mm focal length Acton SpectraPro 2300i triple grating, flat field, double exit monochromator equipped with a photo-multiplier detector (Hamamatsu R3896) and a Princeton Instruments PIMAX II gated intensified CCD camera, using an RB Gen II intensifier, an ST133 controller and a PTG pulser. Signals from the photomultiplier (Hamamatsu R928) were processed by means of a Teledyne LeCroy 604Zi digital oscilloscope (400 MHz, 20 GS s⁻¹).

Light driven catalytic tests for water oxidation were conducted in a home-made glass reactor, equipped with a TROX-ROB10 oxygen probe inserted in the headspace, and connected with a FirestingO2 fiber-optical oxygen meter for real time monitoring of evolved O₂. 15 mL of aqueous buffer was introduced into the reactor, which was then closed and purged under a dark atmosphere with nitrogen for 20 minutes: after purging, the solution was allowed to equilibrate in the dark for 5 minutes and then illuminated with a series of six monochromatic LEDs emitting at 450 nm, photon flux = (8.28 ÷ 0.87) × 10⁻⁸ einstein s⁻¹. The irradiation power of the LEDs was measured with an AvaSpec-2048 Fiber Optic Spectrometer from Avantes.

Conflicts of interest

There are no conflicts to declare.

Acknowledgements

Financial support from Ministero dell'Università e della Ricerca (PRIN 2022 PROMETEO, 2022KPK8WM), by the European Union – Next Generation EU (PRIN2022 PNRR PHOTOCORE, P2022ZSPWF) and from Fondazione Cariparo (Project “SYNERGY”, Ricerca Scientifica di Eccellenza 2018) is greatly acknowledged. We thank the National Recovery and Resilience Plan (NRRP), Mission 4 Component 2 Investment 1.3 – Call for



tender No. 1561 of 11.10.2022 of MUR, funded by the European Union – NextGenerationEU, Project code PE000002 “Network 4 Energy Sustainable Transition – NEST”.

Notes and references

- R. G. Agarwal, S. C. Coste, B. D. Groff, A. M. Heuer, H. Noh, G. A. Parada, C. F. Wise, E. M. Nichols, J. J. Warren and J. M. Mayer, *Chem. Rev.*, 2022, **122**, 1–49.
- R. Tyburski, T. Liu, S. D. Glover and L. Hammarström, *J. Am. Chem. Soc.*, 2021, **143**, 560–576.
- G. A. Parada, Z. K. Goldsmith, S. Kolmar, B. P. Rimgard, B. Q. Mercado, L. Hammarström, S. Hammes-Schiffer and J. M. Mayer, *Science*, 2019, **475**, 471–475.
- M. C. Kessinger, J. Xu, K. Cui, Q. Loague, A. V. Soudackov, S. Hammes-Schiffer and G. J. Meyer, *J. Am. Chem. Soc.*, 2024, **146**, 1742–1747.
- M. Natali, A. Amati, S. Merchiori, B. Ventura and E. Iengo, *J. Phys. Chem. C*, 2020, **124**, 8514–8525.
- M. Natali, A. Amati, N. Demitri and E. Iengo, *Chem.–Eur. J.*, 2021, **27**, 7872–7881.
- E. Benazzi, J. Karlsson, Y. Ben M'Barek, P. Chabera, S. Blanchard, S. Alves, A. Proust, T. Pullerits, G. Izzet and E. A. Gibson, *Inorg. Chem. Front.*, 2021, **8**, 1610–1618.
- M. Kuss-Petermann, M. Oraziotti, M. Neuburger, P. Hamm and O. S. Wenger, *J. Am. Chem. Soc.*, 2017, **139**, 5225–5232.
- A. Pannwitz and O. S. Wenger, *Chem. Commun.*, 2019, **55**, 4004–4014.
- A. Dey, N. Ghorai, A. Das and H. N. Ghosh, *J. Phys. Chem. B*, 2020, **124**, 11165–11174.
- T. F. Markle, J. W. Darcy and J. M. Mayer, *Sci. Adv.*, 2018, **4**, eaat5776.
- P. R. D. Murray, J. H. Cox, N. D. Chiappini, C. B. Roos, E. A. McLoughlin, B. G. Hejna, S. T. Nguyen, H. H. Ripberger, J. M. Ganley, E. Tsui, N. Y. Shin, B. Koronkiewicz, G. Qiu and R. R. Knowles, *Chem. Rev.*, 2022, **122**, 2017–2291.
- P. Franceschi, E. Rossin, G. Goti, A. Scopano, A. Vega-Penalosa, M. Natali, D. Singh, A. Sartorel and L. D. Amico, *J. Org. Chem.*, 2023, **88**, 6454–6464.
- T. Bortolato, G. Simionato, M. Vayer, C. Rosso, L. Paoloni, E. M. Benetti, A. Sartorel, D. Lebcœuf and L. Dell'Amico, *J. Am. Chem. Soc.*, 2023, **145**, 1835–1846.
- Y. Yang, G. A. Volpato, E. Rossin, N. Peruffo, F. Tumbarello, C. Nicoletti, R. Bonetto, L. Paoloni, P. Umari, E. Colusso, L. Dell'Amico, S. Berardi, E. Collini, S. Caramori, S. Agnoli and A. Sartorel, *ChemSusChem*, 2023, e202201980.
- B. P. Sullivan, D. J. Salmon and T. J. Meyer, *Inorg. Chem.*, 1978, **17**, 3334–3341.
- S. W. Gersten, G. J. Samuels and T. J. Meyer, *J. Am. Chem. Soc.*, 1982, **104**, 4029–4030.
- M. Schulze, V. Kunz, P. D. Frischmann and F. Würthner, *Nat. Chem.*, 2016, **8**, 576–583.
- M. A. Hoque, M. Gil-Sepulcre, A. de Aguirre, J. A. A. W. Elemans, D. Moonshiram, R. Matheu, Y. Shi, J. Benet-Buchholz, X. Sala, M. Malfois, E. Solano, J. Lim, A. Garzón-Manjón, C. Scheu, M. Lanza, F. Maseras, C. Gimbert-Suriñach and A. Llobet, *Nat. Chem.*, 2020, **12**, 1060–1066.
- R. Matheu, P. Garrido-Barros, M. Gil-Sepulcre, M. Z. Ertem, X. Sala, C. Gimbert-Suriñach and A. Llobet, *Nat. Rev. Chem.*, 2019, **3**, 331–341.
- L. Duan, F. Bozoglian, S. Mandal, B. Stewart, T. Privalov, A. Llobet and L. Sun, *Nat. Chem.*, 2012, **4**, 418–423.
- R. Matheu, M. Z. Ertem, J. Benet-Buchholz, E. Coronado, V. S. Batista, X. Sala and A. Llobet, *J. Am. Chem. Soc.*, 2015, **137**, 10786–10795.
- A. Sartorel, M. Carraro, G. Scorrano, R. De Zorzi, S. Geremia, N. D. McDaniel, S. Bernhard and M. Bonchio, *J. Am. Chem. Soc.*, 2008, **130**, 5006–5007.
- Y. V. Geletii, B. Botar, P. Kögerler, D. A. Hillesheim, D. G. Musaev and C. L. Hill, *Angew. Chem., Int. Ed.*, 2008, **47**, 3896–3899.
- F. M. Toma, A. Sartorel, M. Iurlo, M. Carraro, P. Parisse, C. MacCato, S. Rapino, B. R. Gonzalez, H. Amenitsch, T. Da Ros, L. Casalis, A. Goldoni, M. Marcaccio, G. Scorrano, G. Scoles, F. Paolucci, M. Prato and M. Bonchio, *Nat. Chem.*, 2010, **2**, 826–831.
- S. X. Guo, Y. Liu, C. Y. Lee, A. M. Bond, J. Zhang, Y. V. Geletii and C. L. Hill, *Energy Environ. Sci.*, 2013, **6**, 2654–2663.
- M. Natali, M. Orlandi, S. Berardi, S. Campagna, M. Bonchio, A. Sartorel and F. Scandola, *Inorg. Chem.*, 2012, **51**, 7324–7331.
- Y. V. Geletii, Z. Huang, Y. Hou, D. G. Musaev, T. Lian and C. L. Hill, *J. Am. Chem. Soc.*, 2009, **131**, 7522–7523.
- G. A. Volpato, M. Marasi, T. Gobatto, F. Valentini, F. Sabuzi, V. Gagliardi, A. Bonetto, A. Marcomini, S. Berardi, V. Conte, M. Bonchio and S. Caramori, *Chem. Commun.*, 2020, **56**, 2248–2251.
- T. Gobatto, F. Rigodanza, E. Benazzi, P. Costa, M. Garrido, A. Sartorel, M. Prato and M. Bonchio, *J. Am. Chem. Soc.*, 2022, **144**, 14021–14025.
- M. Bonchio, Z. Syrgiannis, M. Burian, N. Marino, E. Pizzolato, K. Dirian, F. Rigodanza, G. A. Volpato, G. La Ganga, N. Demitri, S. Berardi, H. Amenitsch, D. M. Guldi, S. Caramori, C. A. Bignozzi, A. Sartorel and M. Prato, *Nat. Chem.*, 2019, **11**, 146–153.
- J. Fielden, J. M. Sumliner, N. Han, Y. V. Geletii, X. Xiang, D. G. Musaev, T. Lian and C. L. Hill, *Chem. Sci.*, 2015, **6**, 5531–5543.
- H. Song, A. Amati, A. Pannwitz, S. Bonnet and L. Hammarström, *J. Am. Chem. Soc.*, 2022, **144**, 19353–19364.
- Y. Xu, L. Duan, L. Tong, B. Åkermark and L. Sun, *Chem. Commun.*, 2010, **46**, 6506.
- Y. Xu, A. Fischer, L. Duan, L. Tong, E. Gabrielsson, B. Åkermark and L. Sun, *Angew. Chem., Int. Ed.*, 2010, **49**, 8934–8937.
- F. Rigodanza, N. Marino, A. Bonetto, A. Marcomini, M. Bonchio, M. Natali and A. Sartorel, *ChemPhysChem*, 2021, **22**, 1208–1218.
- Y. Liu, S. Guo, A. M. Bond, J. Zhang, Y. V. Geletii and C. L. Hill, *Inorg. Chem.*, 2013, **52**, 11986–11996.



- 38 S. Piccinin, A. Sartorel, G. Aquilanti, A. Goldoni, M. Bonchio and S. Fabris, *Proc. Natl. Acad. Sci. U. S. A.*, 2013, **110**, 4917–4922.
- 39 G. A. Volpato, A. Bonetto, A. Marcomini, P. Mialane, M. Bonchio, M. Natali and A. Sartorel, *Sustainable Energy Fuels*, 2018, **2**, 1951–1956.
- 40 W. P. Jencks, *J. Am. Chem. Soc.*, 1972, **94**, 4731–4732.
- 41 W. Jencks, *Chem. Rev.*, 1972, **72**, 705–718.
- 42 S. Hammes-Schiffer, *J. Am. Chem. Soc.*, 2015, **137**, 8860–8871.
- 43 P. K. Ghosh, B. S. Brunschwig, M. Chou, C. Creutz and N. Sutin, *J. Am. Chem. Soc.*, 1984, **106**, 4772–4783.
- 44 C. T. Lin, W. Böttcher, M. Chou, C. Creutz and N. Sutin, *J. Am. Chem. Soc.*, 1976, **98**, 6536–6544.
- 45 U. S. Akhtar, E. L. Tae, Y. S. Chun, I. C. Hwang and K. B. Yoon, *ACS Catal.*, 2016, **6**, 8361–8369.
- 46 J. Lee, U. Von Gunten and J. H. Kim, *Environ. Sci. Technol.*, 2020, **54**, 3064–3081.
- 47 D. Wang and J. T. Groves, *Proc. Natl. Acad. Sci. U. S. A.*, 2013, **110**, 15579–15584.
- 48 A. Volpe, C. Tubaro, M. Natali, A. Sartorel, G. W. Brudvig and M. Bonchio, *Inorg. Chem.*, 2019, **58**, 16537–16545.
- 49 C. Chiorboli, M. T. Indelli, M. A. R. Scandola and F. Scandola, *J. Phys. Chem.*, 1988, **92**, 156–163.

